Brittle Ductile Transition in Carbon Nanotube Bundles

Charles F. Cornwell, Jeffrey B. Allen, Charles P. Marsh, Thomas A. Carlson, Peter B. Stynoski,
Bradley A. Newcomb, Benjamin Masters, Robert M. Ebeling, and Charles R. Welch
U.S. Army Engineer Research and Development Center, MS, USA, charles.f.cornwell@usace.army.mil

ABSTRACT

The superior strength and stiffness of carbon nanotubes (CNTs) make them attractive for many structural applications. While the strength and stiffness of CNTs are extremely high, to date, fibers of aligned CNTs have been found to be far weaker than the constituent CNTs. The intermolecular interactions between the CNTs in the fibers are governed by weak van der Waals forces resulting in slippage between CNTs that occurs at tensions well below the breaking strength of the CNTs. Both theoretical and experimental studies show that introducing chemical bonds between the CNTs increases load transfer and prevents the CNTs from slipping.

Keywords: carbon nanotubes, molecular simulation, mechanical properties, nanofibers, load transfer

1 INTRODUCTION

Krishnan *et al.* [1] measured the Young's modulus of isolated CNTs by measuring the amplitude of their intrinsic thermal vibrations using transmission electron microscopy,and found the average value of Young's modulus 1.25 TPa. Haskins et al. [2] used Tight Binding Molecular Dynamics simulations to examine the effects of defects on CNTs and deduced values of Young's modulus and tensile strengths for (5,5) chiral CNTs of 0.95 to 1.15 TPa and 70 to 110 GPa, respectively, for the molecular defects considered. While the strength and stiffness of CNTs can be extremely high, fibers composed of aligned CNTs are far weaker then the constituent CNTs [3-6]. Studies show that the bundles fail because the relatively weak van der Waals forces between molecules allow CNTs to slip past one another before the shear forces between molecules reach the intrinsic breaking strength of the CNTs [3,7-9]. In this paper, we study the use of chemical bonds as an effective mechanism for coupling the superior mechanical properties of the individual CNTs across length scales. The results show an increase in the strength and elastic modulus of the fibers and also reveal a transition from ductile to brittle failure going from fibers with low to higher cross-link counts.

2 BUNDLE CONSTRUCTION

Experimental results indicate that CNTs within a bundle have similar radii and are randomly distributed[10]; i.e., there is no correlation between the z-coordinates of the different tubes, and they most probably have random azimuthal orientations. The digital representations of the fibers were constructed using a random distribution of CNT lengths, with each CNT given a random rotation about its longitudinal axis between 0 and 2π. The longitudinal axes of the fibers were initially aligned parallel to the z-axis. The strands consisted of parallel (5,5) CNTs placed end to end arranged parallel to one another with a gap of 3.33Å between CNTs in the strands (Fig. 1). Each bundle had 19 strands arranged in an HCP configuration (Fig. 2).

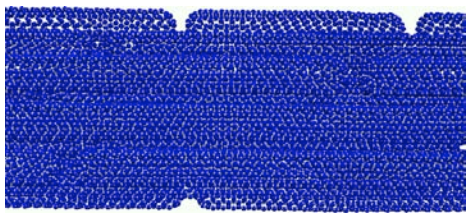

Figure 1 Side view of a section of a CNT bundle with CNTs placed end to end over the length of the bundle.

The position of the cross-link atoms were randomly selected from the volume of the bundle. A check was made to determine if the cross-link atom formed the correct number of nearest neighbor bonds and that it formed bonds between CNTs from two strands. If it did not meet these criteria, it was rejected. The concentration of cross-link atoms is defined as the number of cross-link atoms divided by the number of atoms in the bundle expressed as a percentage.

The simulations had periodic boundary conditions in the three Cartesian dimensions. The system size in the x-y plane was large enough to prevent any interaction across the boundary for atoms in the bundle. A Berendsen thermostat was applied to all the atoms to minimize the heat conduction problem pointed out in Berendsen et al. [11] and Mylvaganam and Zhang [12]. The simulations were run at a temperature of 300 K.

The stress tensor was calculated using:

$$< S_{ij} >= \frac{\sum_{k}^{N} m_k v_{k_i} v_{k_j}}{V} + \frac{\sum_{k}^{N} r_{k_i} f_{k_j}}{V} \quad (1)$$

The first term of Eq. (1) is the kinetic energy tensor, and the second term is the virial stress tensor. *N* is the number of atoms in the system, and the Cartesian coordinates are

designated by i and j = x,y,z. The variables m_k, v_k, r_k, and f_k, are the mass, velocity, position, and force, respectively, for atom k, and V is the volume of the bundle. Here, the volume of the bundle is calculated using the length of the bundle times its cross section. The area of a regular hexagon that encloses the strands of the bundle is used to define the fiber's cross-sectional area. Figure 2 shows the cross section of the fibers with the cross-link atoms forming chemical bonds between the CNTs. The cross-section of the bundle is considered constant throughout the simulation.

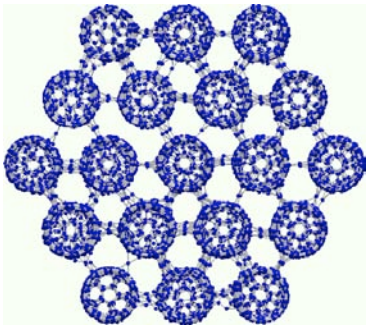

Figure 2 Cross section of bundle with cross-link atoms forming chemical bonds between the CNTs.

3 SIMULATION

Because the fibers were constructed using CNTs with random orientations, random distribution of lengths, and a random distribution of cross-link atoms, one would expect variations in the mechanical properties of the fibers caused by the random method of bundle construction. Figure 3 shows the stress-strain curves for eight statistically equivalent fibers. The fibers were 4000Å long and were constructed using CNTs with an average length of 1000Å. The standard deviation in the tube length was 200Å, and they all had a cross-link concentration of about 0.225 percent.

The elastic modulus was calculated over the linear portion of the stress-strain curves, hence is an initial or tangent modulus. The point of maximum stress was used to determine the tensile strength of the fibers. While there are some variations in the stress-strain curves in Fig. 3, the simulations produce consistent and reproducible results for statistically equivalent fibers. The average maximum stress for the eight simulations is 33.467 GPa with a standard deviation of 2.495 GPa. This represents a standard deviation of 7.46 percent of the average maximum stress. The eight simulations had an average initial elastic modulus of 586.434 GPa with a standard deviation of 14.743 GPa, representing a standard deviation of 2.51 percent of the average initial modulus.

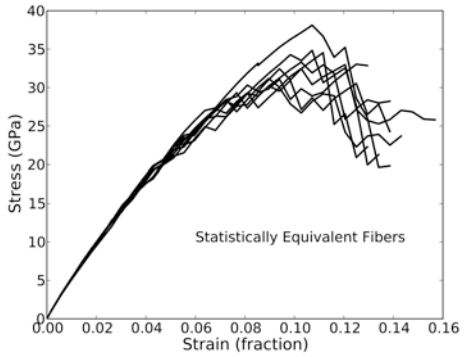

Figure 3 Stress-strain curve for eight statistically equilvalent fibers. A different seed was used for the random number generator used to construct the CNTs with an average length of 1000 Å and a standard deviation of 200 Å. Also, a different seed was used to select the postion of the cross-link atoms.

4 RESULTS

A series of simulations were run to investigate the effect of CNT length and cross-link distribution on the tensile response of parallel-aligned CNT fibers. Results of the stress-strain calculations are presented in Fig. 4. The elastic modulus and tensile strength for fibers with initial lengths of 4000Å with cross-link concentrations that ranged from 0.113 - 0.451 percent. The plots of lower to higher cross-link concentrations run from lower to higher stress for each cross-link concentration considered. The maximum tensile strength of 50.24 GPa calculated for the bundle with an initial percentage of cross-links of 0.394, and the maximum elastic modulus 629.17 GPa was calculated for the bundle with an initial percentage of cross-links of 0.451. The results of the stress-strain calculations presented in Fig. 4 also reveal a transition from ductile to brittle failure going from bundles with low to higher cross-link counts. A detailed understanding of the bundle postyield response is required to optimize the strength and elastic modulus of fibers and to prevent brittle failure. Figure 4 shows a transition from ductile to brittle between cross-link contrations of 0.225. and 0.281 percent.

The stress tensor was calculated by averaging Eq. (1) over 20 picoseconds (ps). If the difference in the stress between two consecutive stress calculations was below a given threshold, the stress was considered at equilibrium and the process continued. This provided a feedback loop that effectively resulted in a variable strain rate, based on simulation conditions, that gave the bundle time to respond to bond breaking, defect formation and migration, slipping or failure of the CNTs, and the resulting structural changes that took place in the bundle from these processes.

Strain was applied to the fibers by increasing the length of the bundle in small increments and allowing the stress to equilibrate between strain increments. Figure 5 shows the

time evolution of the stress and strain for two strain increments. The stress was then allowed to approach equilibrium after each strain increment. At time *t = 0* ps, the strain was increased at a rate of 2.0 E8(s^{-1}) for 10 ps increasing the strain by 0.002 (fraction). At *t =150* ps, the strain was increased at a rate of 2.0 E8 (s^{-1}) for 20 ps, increasing the strain by 0.004 (fraction). In both cases, the strain was held constant for a period after each increase in strain to allow the stress to equilibrate.

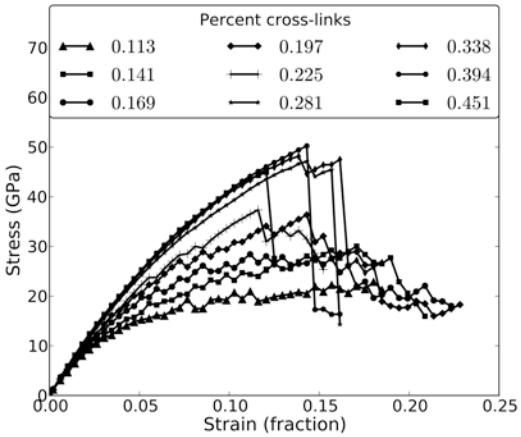

Figure 4 Stress-strain curves for a bundle 4000Å long with the percent cross-links ranging from 0.125 to 0.500.

The results in Fig. 6 show the time evolution of the stress and strain for two 4000Å fibers. The average length and standard deviation of the CNTs in both fibers are 1000Å and 200Å, respectively. The number of cross-links per CNT in the two fibers differs. The initial percentage of cross-links is 0.250 and 0.750 or an average of 26.8 and 80.4 cross-links for each core CNT, respectively. The plot of the stress and strain data in Fig. 6 is the time average of the stress and strain at 10-ps intervals.

In Fig. 6 the bundle with 0.750 percent cross-link concentration reached a maximum stress of 53.99 GPa at a strain of 0.148 in 1.68 ns. At 1.77 ns and a strain of 0.157, the bundle began to fail. At that point, the average strain held constant and the stress decreased until the bundle broke. Recall that displacement boundary conditions were used in the simulations. While the average strain in the bundle was holding constant, inside the bundle, bonds were failing; and the average internal stress was decreasing. The bundle stress never stabilized once the bundle exceeded a strain of 0.177. In a macroscopic analogy, this is brittle failure.

On the other hand, plot 0.250 in Fig. 6 reached a maximum stress of 38.42 GPa at a strain of 0.121 in 3.35 ns. At that point, the bundle began to fail, and the strain was held constant for 0.71 ns before the bundle stress stabilized. The stress continued to decrease with increasing strain, but the bundle did not break and was able to support stress up to a strain of 0.157, where the simulation was terminated. In a macroscopic analogy, this is equivalent to ductile behavior.

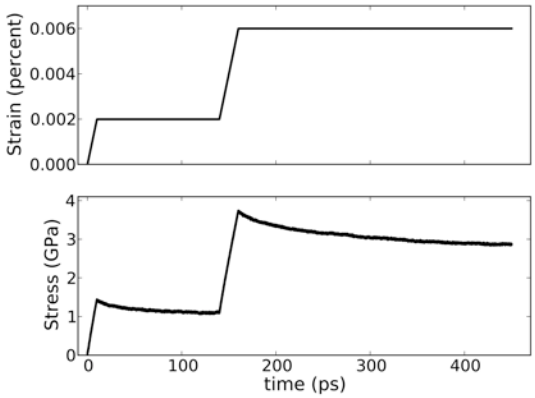

Figure 5 Time evolution for the stress and strain for one of the bundle runs. The strain is increased in 0.004 increments and then allowed to equilabrate before increasing the strain. The stress and strain are recorded at the point where the stress reaches equilibration.

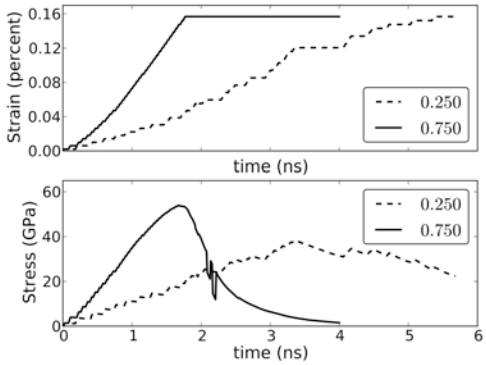

Figure 6 Time evolution of the stress and strain for a 4000Å bundle. The average sength of the CNTs in the bundle is 1000Å with a standard deviation of 200Å. The initial percentages of cross-links in the fibers are 0.25 and 0.75.

Figures 7 and 8 capture snapshots of the postyield results of bundle failure. The simulations indicate that failure in all fibers begins when the bundle responds to bond breaking, defect formation, and slipping or failure of the CNTs. This results in a release of stress and structural changes in the bundle. If the resulting structure of the bundle is able to support the residual stress, the stress stabilizes. Otherwise, the bundle will fail again, and the process is repeated until the stress stabilizes or the bundle breaks.

Generally, the fibers with shorter CNTs and lower concentrations of cross-links fail at the cross-links. Apparently, failure of a cross-link results in less damage to the CNTs and thus results in little damage to the bundle. In Fig. 7, the 4000Å bundle with a 0.113 percentage of cross-

links was able to support a load out to a strain of 0.23, where the simulation was terminated. It can be seen that some of the CNTs are damaged, but other CNTs slip past one another when the C-C bonds of the cross-link atoms brake. In general, this tends to produce less damage to the bundle, and it is still able to support the residual stress.

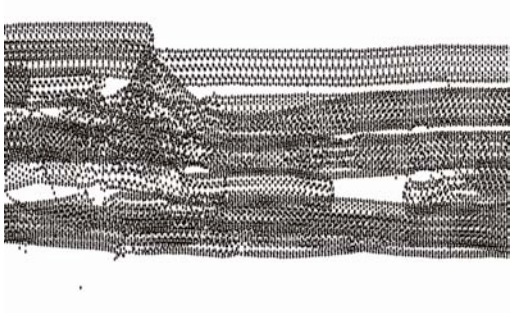

Figure 7 Bundle with 0.113 percent cross-link atoms. Fibers with lower cross-link concentrations tend to achieve lower maximum stress but produce less damage to the bundle during failure. As a result, the failure tends to be more ductile.

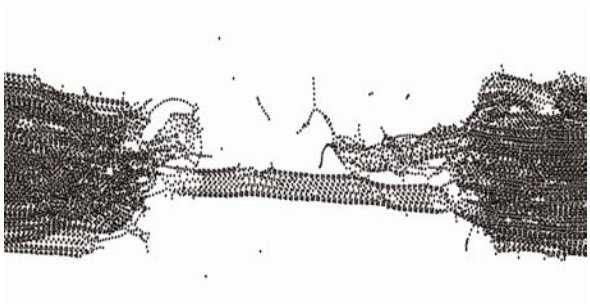

Figure 8 Bundle with 0.394 percent cross-limk atoms. Fibers with higher cross-link concentrations tend to achieve higher maximum stress but produce substantial damage to the bundle during failure. As a result, the failure tends to be brittle.

On the other hand, the CNTs tend to fail in fibers (Fig. 8) with longer CNTs and higher concentrations of cross-links. A CNT failure damages the bundle and makes it less likely that it will be able to support the residual stress in the bundle.

5 CONCLUSION

These results indicate that cross-links between CNTs promote load transfer while allowing them to retain the majority of their structural integrity. The simulations show an increase in the elastic modulus, critical strain, and yield strength with an increase in the average CNT length and cross-link concentrations. Precise control of the cross-link concentration and distribution may allow the maximum bundle strength and elastic modulus to be achieved while producing favorable postyield behavior. Ultimately, the ability to produce CNT fibers with a minimum number of defects while optimizing the number and distribution of cross-links will play a major roll in determining the properties of CNT fibers.

6 ACKNOWLEDGMENTS

This study gratefully acknowledges funding support from the U.S. Army Engineer Research and Development Center Research Program "Molecular-Designed Carbon Nanotube Filaments, Membranes, and Coatings," the HPC Challenge Project "Molecular Dynamics Simulations to Underpin the Design and Development of High-Performance Carbon-Nanotube-Based Filaments, Membranes, and Coatings," and allocation of computer time from the Department of Defense High Performance Computing Modernization Program.

References

[1] A. Krishnan, E. Dujardin, T. W. Ebbesen, P. N. Yianilos, and M. M. J. Treacy, Phys. Rev. B **58**, 14013 (1998).

[2] R. W. Haskins, R. S. Maier, R. M. Ebeling, C. P. Marsh, D. L. Majure, A. J. Bednar, C. R. Welch, B. C. Barker, and D. T. Wu, J. Chem. Phys. **127**, 074708 (2007).

[3] D. Qian, W. K. Liu, and R. S. Ruoff, Compos. Sci. Technol. **63**, 1561 (2003)

[4] L. M. Ericson, H. Fan, H. Peng, V. A. Davis, W. Zhou, J. Sulpizio, Y. Wang, R. Booker, J. Vavro, C. Guthy, A. N. G. Parra-Vasquez, M. J. Kim, S. Ramesh, R. K. Saini, C. Kittrel, G. Lavin, H. Schmidt, W. W. Adams, W. E. Billps, M. Pasquali, W. F. Hwang, R. H. Hauge, J. E. Fischer, R. E. Smalley, Science **305**, 1447 (2003).

[5] K. Koziol, J. Vilatela, A. Moisala, M. Motta, P. Cunniff, M. Sennett, and A. Windle, Science **318**, 1892 (2007).

[6] S. Zhang, L. Zhu, M. L. Minus, H. G. Chae, S. Jagannathan, C.-P. Wong, J. Kowalik, L. B. Roberson, and S. Kumar, J. Mater. Sci. **43**, 4356 (2008).

[7] D. A. Walters, L. M. Ericson, M. J. Casavant, J. Liu, D. T. Colbert, K. A. Smith, and R. E. Smalley, Appl. Phys. Lett. **74**, 3803 (1999).

[8] M.-F. Yu, B. I. Yakobson, and R. S. Ruoff, J. Phys. Chem. B **104**, 8764 (2000a).

[9] M.-F. Yu, O. Lourie, M. J. Dyer, K. Moloni, T. F. Kelly, and R. S. Ruoff, Science **287**, 637 (2000b).

[10] A. Thess, R. Lee, P. Nikolaev, H. Dai, P. Petit, J. Robert, C. Xu, Y. H. Lee, S. G. Kim, A. G. Rinzler, D. T. Colbert, G. E. Scuseria, D. Tomanek, J. E. Fischer, and R. E. Smalley, Science **273**, 483 (1996).

[11] H. J. C. Berendsen, J. P. M. Postma, W. F. van Gunsteren, A. DiNola, and J. R. Haak, J. Chem. Phys. **81**, 3684 (1984).

[12] K. Mylvaganam and L. C. Zhang, Carbon **42**, 2025 (2004).